

Photoionisation loading of large Sr⁺ ion clouds with ultrafast pulses

S. Removille · R. Dubessy · Q. Glorieux · S. Guibal ·
T. Coudreau · L. Guidoni · J.-P. Likforman

Received: 27 January 2009 / Revised version: 8 June 2009 / Published online: 8 August 2009
© Springer-Verlag 2009

Abstract This paper reports on the use of ultrafast pulses for photoionisation loading of singly-ionised strontium ions in a linear Paul trap. We take advantage of an autoionising resonance of Sr neutral atoms to form Sr⁺ by two-photon absorption of femtosecond pulses at a wavelength of 431 nm. We compare this technique to electron-bombardment ionisation and observe several advantages of photoionisation. It actually allows for the loading of a pure Sr⁺ ion cloud in a low radio-frequency voltage amplitude regime. In these conditions, up to 4×10^4 laser-cooled Sr⁺ ions were trapped.

PACS 32.80.Fb · 32.80.Rm · 37.10.Ty

1 Introduction

Samples of laser-cooled ions confined in electromagnetic traps play a prominent role in several domains related to atomic physics: quantum information [1, 2], metrology [3], quantum optics [4–6]. The traditional method used to load an ion trap with the desired species is to create the ions directly inside the trapping region by electron bombardment (EB) of a neutral atomic beam. As already underlined by several groups [7–10], this technique, while very flexible because it applies to any atomic (and molecular) specie, has several serious drawbacks. Firstly, the electron beam may

charge some insulator present near the trap affecting the trapping potential with a slowly varying non-controlled electric field. This situation induces excess micro motion which is thought to lead to increased heating. The slowly varying field must be frequently compensated for, by readjustment of compensation-voltages [9, 10]. Secondly, the vacuum quality of the setup is deteriorated by the presence of a hot filament near the trap. Finally, the very small cross section of the electron-impact ionisation requires huge atomic fluxes that negatively affect both the vacuum and the electrode surfaces. In recent years, several groups have developed new strategies in order to eliminate these drawbacks: laser ablation [11, 12] and photoionisation. We can distinguish two different photoionisation methods, depending on the excitation path from the neutral atom to the ionised state. In what we will call two-step photoionisation (TSPI) a first narrowband cw laser is tuned on an intermediate transition and the ionisation threshold is attained with a second photon (that can possibly have the same energy). This method needs a non-negligible population in the intermediate level (saturating stabilised laser). Another technique, developed here, consists in using a two-photon transition that directly brings a neutral atom above the ionisation threshold (two-photon photoionisation, TPPI). TPPI requires high peak-power, normally associated with short-pulse lasers with a large spectral width. TSPI has been applied to Mg [7, 13], Ca [7–9, 14], Ba [15], Yb [16, 17], and Sr [10]. It presents the important opportunity of isotope selectivity through the shifts associated to the intermediate transition. Cd⁺ ions have been produced using short pulses [18], taking advantage of the pulse duration of titanium:sapphire (Ti:Sa) sources to efficiently double and quadruple the fundamental frequency. These experimental results are interpreted in terms of TSPI; however, when spectrally-large pulses excite long-lived intermediate states, TPPI might also occur.

S. Removille · R. Dubessy · Q. Glorieux · S. Guibal ·
T. Coudreau · L. Guidoni · J.-P. Likforman (✉)
Laboratoire Matériaux et Phénomènes Quantiques, Université
Paris Diderot et CNRS, UMR 7162, Bât. Condorcet, 75205 Paris
Cedex 13, France
e-mail: jean-pierre.likforman@univ-paris-diderot.fr
Fax: +33-(0)1-57276241

This paper reports on photoionisation loading of Sr^+ in a linear Paul trap based on ultrafast pulses. We demonstrate that TPPI presents indeed several advantages with respect to EB. In particular, it allowed us to selectively load the trap with Sr^+ ions, to explore trapping regimes with low RF voltages, to obtain larger ion clouds and to improve the vacuum quality by lowering the power in the Sr oven. Such a lower atom flux is particularly interesting in the case of micro-fabricated traps because it prevents short-circuits on the electrodes and reduces heating associated with patch potentials [19]. As TPPI is based on femtosecond pulses, the laser spectral width is on the order of several nm. Therefore frequency stabilisation is not necessary and Doppler broadening effects are negligible. Let us also mention that, because of its two-photon character, TPPI has the potential advantage to define a well-localised spatial region for the ion production associated with the waist of the ionising beam [20]. This facilitates the ion creation at the centre of the trap with an initially low potential energy. In the particular case of our trap (atomic beam spread of $\simeq 8$ mm on the trap axis), we compared the theoretical performances of TPPI and TSPI (assuming equivalent ionisation rates) and we found an initial temperature six times lower for TPPI. More generally, for perfectly collimated atomic beams, the expected initial temperature is at least two times lower for TPPI than for TSPI. Finally, from a practical point of view, the TPPI setup presents the advantage of flexibility because the same frequency-doubled tunable ultrafast source can be used for the ionisation of different atomic species.

2 Experimental setup

The level structure of the Sr atom is similar to that of most atoms with two electrons in the outer shell (the relevant levels are represented in Fig. 1a). The 1P_1 intermediate level has been used to implement TSPI technique in Sr [10], following the example of Ca [8] and Yb [16, 17]. In the particular case of the Sr atom, the presence of a $(4d^2 + 5p^2){}^1D_2$ autoionising state that lies above the ionisation threshold is very helpful to increase the photoionisation efficiency. The spectral characteristics of this state have been investigated earlier [21], in particular a cross section of $\simeq 5500$ Mb ($1 \text{ Mb} = 10^{-22} \text{ m}^2$) for the ${}^1P_1 \rightarrow (4d^2 + 5p^2){}^1D_2$ transition has been measured. Such an autoionising state can also be reached from the ground state by two-photon absorption: the $(5s^2){}^0S_0 \rightarrow (4d^2 + 5p^2){}^1D_2$ two-photon transition has a linewidth of 0.7 nm FWHM (due to the short lifetime of the final state) and can be resonantly driven by two photons centred at 431 nm [22]. The strategy of the TPPI loading experiment described in this paper is based on this transition (Fig. 1b).

The neutral atomic beam is produced in an oven placed below the trap. The oven contains a dendritic piece of pure

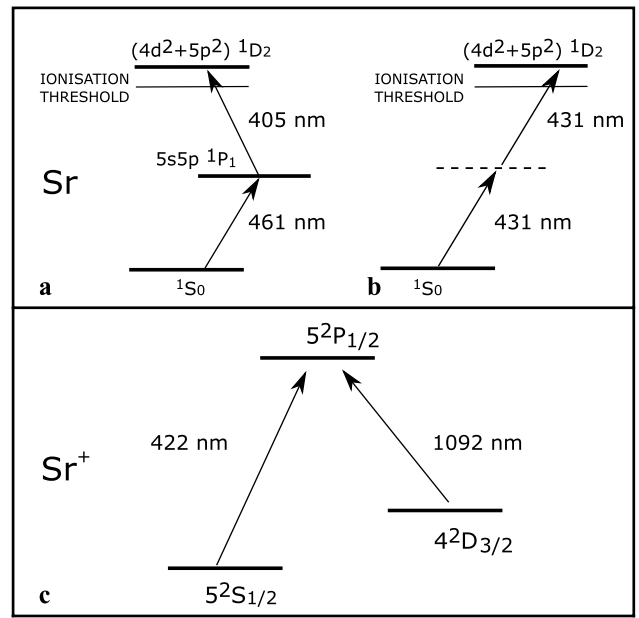
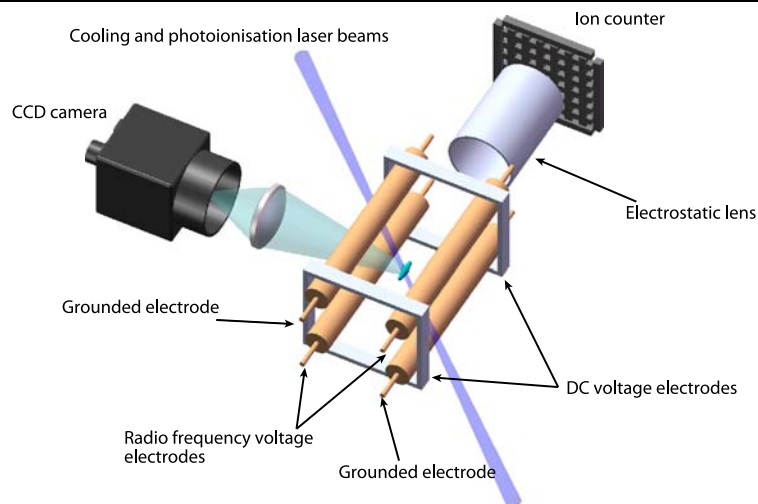


Fig. 1 Relevant energy levels of neutral strontium involved in: **a** two-step photoionisation TSPI; **b** two-photon photoionisation TPPI discussed in this paper. **c** Relevant energy levels of Sr^+ ion involved in Doppler cooling

strontium (Aldrich) heated by a tungsten filament with a maximum operating current of 1.15 A, corresponding to a heating power of 1.3 W. Let us remark that the manipulation of pure Sr under argon atmosphere in a glove box did not produce visible oxidation of the sample. The temperature of the (bare) filament displays an approximate linear dependence on the current and we measured 110°C for 0.8 A and 170°C for 1.2 A. Such measurements have been carried out by recording the I–V characteristics and by taking into account the known dependence of the tungsten resistivity as function of the temperature. In these conditions we expect an Sr partial pressure near the filament roughly in the range 10^{-13} – 10^{-9} mbar [23]. An electron gun based on a thorium tungsten wire allows us to perform EB with a typical electron energy of $\simeq 300$ eV. The photoionising laser source is based on a homemade femtosecond Ti:Sa oscillator that produces 50 fs pulses of 1.5 nJ energy at 862 nm with a repetition rate of 100 MHz. The pulses are frequency doubled in a 0.5 mm thick Beta Barium Borate (BBO) nonlinear crystal. The thickness of the crystal is such that the group velocity mismatch negligibly affects pulse duration. A pulse energy of more than 0.15 nJ is routinely obtained at 431 nm. The beam is directed into the vacuum chamber and focused at the centre of the ion trap by a lens of focal distance 200 mm. The measured photoionising beam size at the waist is $20 \pm 2 \mu\text{m}$, corresponding to a peak intensity of $\simeq 1 \text{ GW/cm}^2$.

Sr^+ ions are trapped in a standard linear Paul trap (see Fig. 2) [24]. Four parallel rod electrodes (diameter 6.35 mm, distance between the centre of the trap and the electrode sur-

Fig. 2 Schematic description of the linear Paul trap setup. Four parallel rod electrodes are used for the rf radial confinement. Two annular end caps separated by 20 mm are used for the longitudinal confinement. The trapped ions can be axially ejected and counted by an electron multiplier. The ion cloud fluorescence resulting from Doppler cooling is recorded on a ccd camera



faces $r_0 = 3.2$ mm) are used for the radio-frequency (rf) radial confinement. A 2.5 MHz rf potential with an amplitude V_{rf} in the range 50–500 V is applied to two of the diagonally opposed electrodes. The remaining two rods are normally grounded but can also be used to resonantly excite the ion motion in the trap (see below). The Sr^+ ion radial movement is defined by a typical secular frequency $\nu_R = 400$ kHz for an applied voltage $V_{\text{rf}} = 500$ V. Two annular “end caps” separated by 20 mm are used for the longitudinal confinement and brought to a static positive voltage ($V_{\text{ec}} = 500$ V). The corresponding axial frequency is $\nu_A = 20$ kHz. The stability parameter q [25] lies within the range 0.09 to 0.45, well below the limit of 0.85. The stability parameter a introduced in the case of linear Paul traps [26, 27], that depends on the end caps voltage, is kept constant at the small value of 10^{-5} . Trapped ions can be detected in a destructive way by an ejection sequence: an asymmetric potential is applied to the end caps that kicks out the cloud along the trap axis through an electrostatic lens towards an electron multiplier. The efficiency of such a process has been estimated to be better than 99% using Simion® software [28]. This detection scheme allows us to perform ion-counting and to analyse the trapped species by performing mass spectrum analysis. A mass spectrum is obtained by measuring the losses induced in successive realisations of the cloud in the presence of a “tickle” sinusoidal excitation applied to two diagonally opposed rods. The result of this parametric excitation is a depletion of the ion signal when the tickle frequency matches an integer fraction of $2\nu_R$ (negative peak in the mass spectrum) [29, 30].

Trapped Sr^+ ions are Doppler cooled using the $^2S_{1/2} \rightarrow ^2P_{1/2}$ optical transition at 422 nm (natural linewidth, $\Gamma/2\pi = 20.2$ MHz, Fig. 1c). This transition is driven using laser light generated by a commercial extended-cavity diode laser (Toptica DL100). A commercial “repumping” fiber laser (Koheras Adjustik Y10) at 1092 nm drives the

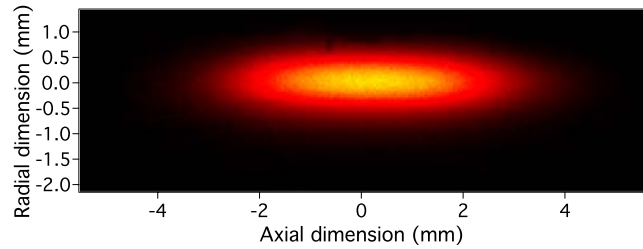


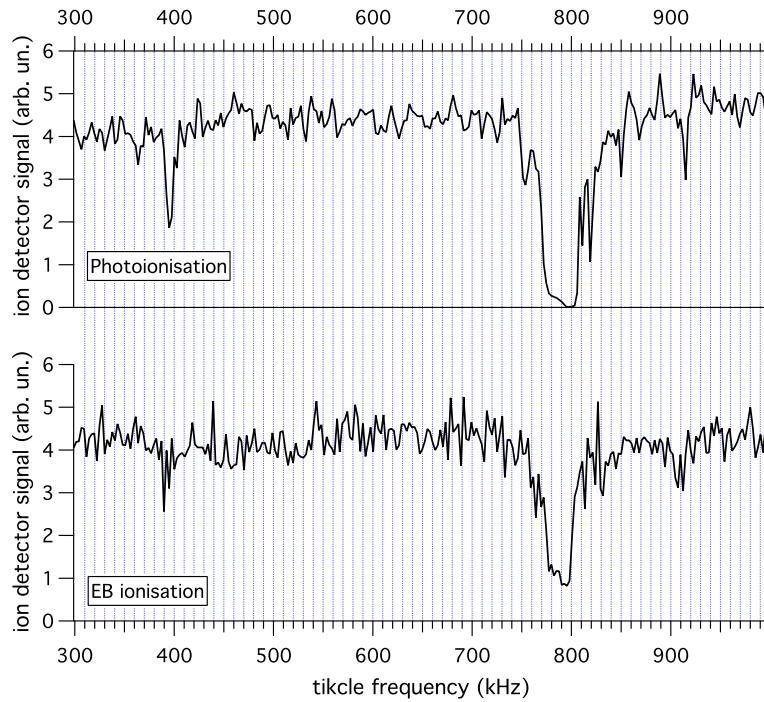
Fig. 3 Fluorescence image at 422 nm of a trapped ion cloud (2 mm length and 200 μm width, FWHM) containing 3×10^4 Sr^+ ions ($V_{\text{rf}} = 130$ V, $V_{\text{ec}} = 500$ V)

$^2D_{3/2} \rightarrow ^2P_{1/2}$ transition to avoid the accumulation of the ions (optical pumping) into the metastable $^2D_{3/2}$ state. Let us mention that this setup allows us to perform both the measurement of the ion fluorescence, useful for optimising the cooling phase, and the precise evaluation of the number of trapped ions by ejection and ion-counting detection. An example of a fluorescence image of a large cloud (2 mm length and 200 μm width, FWHM) containing 3×10^4 Sr^+ ions is shown in Fig. 3. In order to remove background light from the images, we perform spatial filtering in an intermediate object plane through a 10 mm long and 0.5 mm wide slit and we filter both in polarisation and wavelength (interferential filter) the detected photons.

3 Results

In a first experiment, we performed mass spectrum analysis of the trapped ions produced either by EB or by TPPI. Typical mass spectra corresponding to these techniques are shown on Fig. 4. Basically two main peaks associated with Sr^+ are expected and observed, corresponding to a tickle frequency of $2\nu_R$ and ν_R (negative peaks in the mass spectrum). This frequency (400 kHz for the experimental conditions of Fig. 4) depends on the trap potentials and the

Fig. 4 Comparison of mass spectra of the trapped ions produced either by electron-beam or by photoionisation for $V_{rf} = 500$ V. The two main peaks associated with Sr^+ are observed for a tickle frequency of $2\nu_R$ and ν_R (negative peaks in the mass spectrum). The two experiments are carried out so that the initially trapped ion numbers are identical. The dark count falls to zero since the probability for an un-trapped spurious ion to reach the detector during the integration time is negligible



ion mass. The main difference between the two spectra is the value of the peak contrast. The contrast of the saturated peak at $2\nu_R$ gives us information about the proportion of Sr^+ ions in the trap. TPPI produces a contrast of 100%, indicating that a pure Sr^+ cloud is obtained, compared to 66% in the case of EB for which other ion species are also produced (among these contaminants, we identified Ar^+ , Cu^+ and water). Since the ionisation rate as a function of the ionising beam intensity shows a quadratic dependence (Fig. 5), we conclude that the ionisation process is actually based on the expected two-photon absorption. The reported rates are obtained by performing several load–eject cycles for different short loading times τ (see below), and by extracting the slope of the linear behaviour by a fit. The error bars represent the average variance as extracted by the fit procedure. The loading rate is expected to saturate when the probability of two-photon absorption for each atom crossing the interaction region is on the order of unity. The intensity range in which this saturation occurs depends on both the two-photon ionisation cross section σ_{tp} for the $(5s^2)^0S_0 \rightarrow (4d^2 + 5p^2)^1D_2$ transition and the photoionising pulse duration. A rough estimate (i.e. that does not take into account the spectrum of the femtosecond pulses) [31] gives $\sigma_{tp} \simeq 10^4$ GM (1 GM = 10^{-50} cm 4 s). By considering a thermal velocity of 200 m/s, an atom interacts with $\simeq 10$ laser pulses in the interaction region and the saturating peak intensity is on the order of $\simeq 100$ GW/cm 2 . In this high-intensity regime, we expect the loading rate to be limited by the density of Sr atoms.

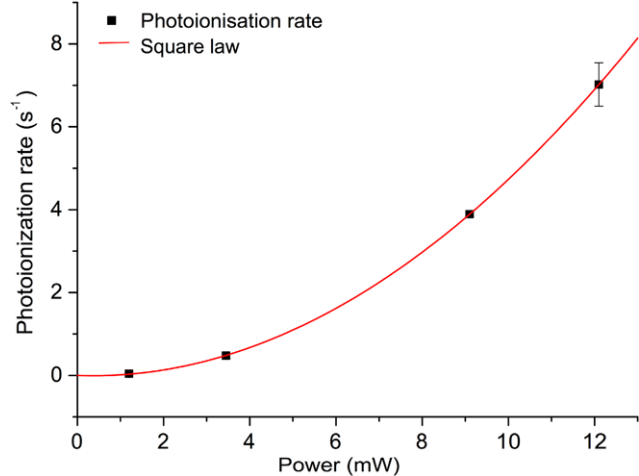


Fig. 5 Photoionisation rate as function of the average power of the ionisation beam obtained for $V_{rf} = 130$ V and $V_{ec} = 500$ V. An excellent quadratic law is observed, as expected for a two-photon absorption process

In a second experiment, we compared the loading times and the maximum number of trapped ions in the two cases of EB and TPPI. The experiment is performed as follows: we turn-on the electron gun or the photoionising beam at time $t = 0$; after a certain time τ , we turn off the laser cooling and eject the loaded ions towards the ion counter. Laser cooling is stopped in the ejection phase to avoid spurious losses induced by damping. We show in Fig. 6a the number of trapped ions, as a function of τ , obtained using the two techniques. In both cases, saturation in the number of

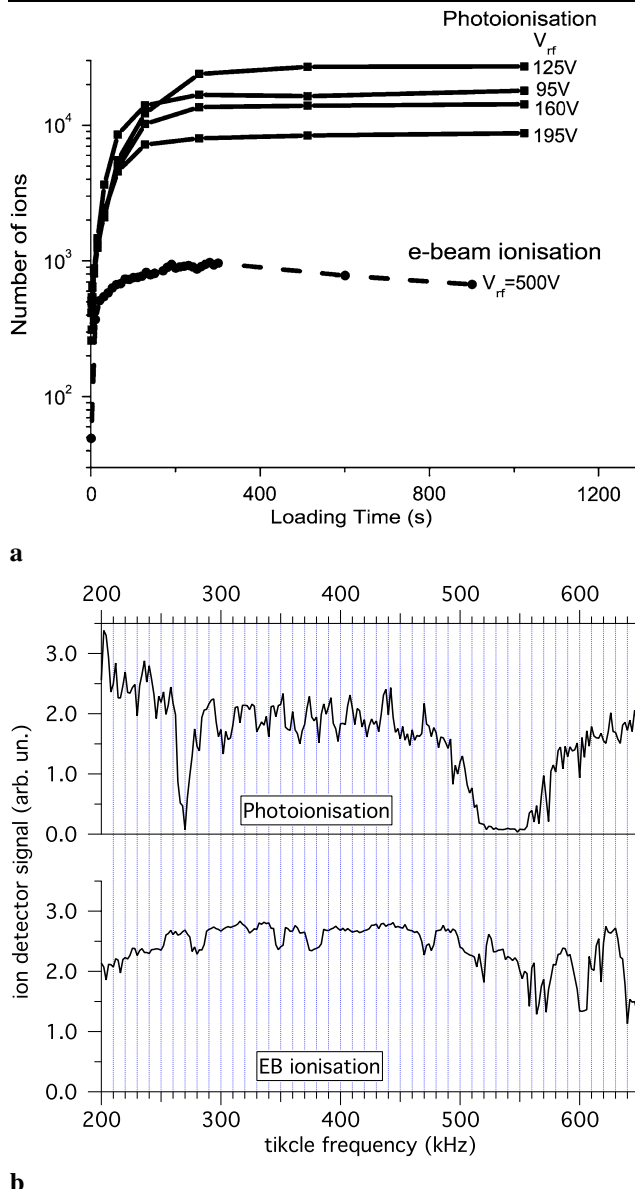


Fig. 6 **a** Number of trapped ions as function of the loading time. In the case of photoionisation, the curves corresponding to several V_{rf} are traced. **b** Mass spectra of the trapped ions produced either by electron-beam (solid curve) or by photoionisation (dashed curve) for $V_{\text{rf}} = 350$ V. All the data are obtained for $V_{\text{ec}} = 500$ V

trapped ions is reached within a few tens of seconds. However, only TPPI allowed us to create pure Sr^+ clouds containing a large number of ions: the EB technique saturates around 1000 trapped ions. In fact, with TPPI an optimum of 4×10^4 trapped Sr^+ ions is obtained for $V_{\text{rf}} = 125$ V. In the case of EB it is impossible to explore the same range for the parameter V_{rf} without affecting the sample purity, since too many spurious ionic species, of mass lower than Sr, are produced and trapped at low V_{rf} . This effect is clearly visible in the mass spectra of Fig. 6b obtained with the two techniques in an intermediate regime ($V_{\text{rf}} = 350$ V). Therefore, in our

case of a non-crystallised regime, the possibility to work at a low V_{rf} is crucial in order to obtain a large number of trapped ions. We interpret this result in terms of a rf-heating process that increases with V_{rf} [32]. In this situation, and in the presence of laser cooling, the ion density depends on the balance between cooling and heating. A maximum density is then achievable by minimising V_{rf} (i.e. the rf heating) within the stability region. But the total number of trapped ions also depends on the volume of the trap that is imposed by V_{rf} and V_{ec} . Numerical simulations carried-out using Simion® software [28] allowed us to estimate the trap volume as a function of V_{rf} for $V_{\text{ec}} = 500$ V. An optimum (maximum) volume is obtained for $V_{\text{rf}} = 180$ V, slightly larger than the experimental value that maximises the total number of trapped ions. Let us note that for low-temperature samples (e.g. in crystallised regime) the ion density increases by increasing V_{rf} , provided that the rf heating remains low enough to prevent the melting of the crystal.

We also observed that, when working in the regime of relatively high V_{rf} , that is optimal for EB ($V_{\text{rf}} = 500$ V), $1100 \pm 5\%$ ions can be trapped by EB to be compared to $1200 \pm 5\%$ ions obtained by photoionisation. This small discrepancy might be explained by space charge effects due to electrons that can perturb the trap electrostatic potential. Let us also finally remark that the selectivity of the TPPI technique allowed us to load pure Sr^+ clouds in the trap at very low oven temperatures (on the order of 120°C), contrary to the case of EB (on the order of 165°C). As mentioned above, this lower temperature implies a vapour pressure reduction of several orders of magnitude.

4 Conclusion

We demonstrated the loading of Sr^+ in a linear Paul trap using two-photon absorption of ultrafast pulses centred at 431 nm. We compared this technique to the electron-bombardment loading and observed several advantages, already mentioned in previous experiments concerning other species or other photo-excitation paths. In particular, this technique allowed us to selectively load pure Sr^+ clouds, to explore trapping regimes with low RF voltages, to obtain large cooled-ion clouds, and to improve the vacuum quality by lowering the power in the Sr oven. Concerning this last point, it has been possible to reduce the expected Sr partial pressure near the oven filament by roughly 4 orders of magnitude. Our results have been obtained with a home-made femtosecond source that delivers relatively low energy pulses. We expect an improvement of two orders of magnitudes in the photoionisation rate in the case of commercially available Ti:Sa oscillators delivering routinely 10 nJ per pulse. Let us finally mention that the trapping of up to 4×10^4 cooled Sr^+ ions is an important step towards the realisation of an ion-based quantum memory [33].

Acknowledgements We thank P. Lepert for technical support. The authors would also like to thank M. Joffre for the loan of the femtosecond oscillator. This work was supported by ANR “jeunes chercheuses et jeunes chercheurs” research contract JC05_61454.

References

1. H. Häffner, C.F. Roos, R. Blatt, Phys. Rep. **469**, 155 (2008)
2. R. Blatt, D. Wineland, Nature **453**, 1008 (2008)
3. P. Gill, Metrologia **42**, S125–S137 (2005)
4. G.R. Guthöhrlein, M. Keller, K. Hayasaka, W. Lange, H. Walther, Nature **414**, 49 (2001)
5. J. Eschner, C. Raab, F. Schmidt-Kaler, R. Blatt, Nature **413**, 495 (2001)
6. P. Herskind, A. Dantan, M.B. Langkilde-Lauesen, A. Mortensen, J.L. Sørensen, M. Drewsen, Appl. Phys. B **93**, 373–379 (2008)
7. N. Kjærgaard, L. Hornekær, A.M. Thommesen, Z. Videsen, M. Drewsen, Appl. Phys. B **71**, 207–210 (2000)
8. S. Gulde, D. Rotter, P. Barton, F. Schmidt-Kaler, R. Blatt, W. Hogervorst, Appl. Phys. B **73**, 861–863 (2001)
9. D.M. Lucas, A. Ramos, J.P. Home, M.J. McDonnell, S. Nakayama, J.-P. Stacey, S.C. Webster, D.N. Stacey, A.M. Steane, Phys. Rev. A **69**, 012711 (2004)
10. M. Brownnutt, V. Letchumanan, G. Wilpers, R.C. Thompson, P. Gill, A.G. Sinclair, Appl. Phys. B **87**, 411–415 (2007)
11. R.J. Hendricks, D.M. Grant, P.F. Herskind, A. Dantan, M. Drewsen, Appl. Phys. B **88**, 507–513 (2007)
12. D.R. Leibrandt, R.J. Clark, J. Labaziewicz, P. Antohi, W. Bakr, K.R. Brown, I.L. Chuang, Phys. Rev. A **76**, 055403 (2007)
13. D.N. Madsen, S. Balslev, M. Drewsen, N. Kjærgaard, Z. Videsen, J.W. Thomsen, J. Phys. B **33**, 4981–4988 (2000)
14. A. Mortensen, J.T. Lindballe, I.S. Jensen, P. Staanum, D. Voigt, M. Drewsen, Phys. Rev. A **69**, 042502 (2004)
15. A.V. Steele, L.R. Churchill, P.F. Griffin, M.S. Chapman, Phys. Rev. A **75**, 053404 (2007)
16. K. Hosaka, S.A. Webster, P.J. Blythe, A. Stannard, D. Beaton, H.S. Margolis, S.N. Lea, P. Gill, IEEE Trans. Instrum. Meas. **54**, 759–762 (2005)
17. Chr. Balzer, A. Braun, T. Hannemann, Chr. Paape, M. Ettler, W. Neuhauser, Chr. Wunderlich, Phys. Rev. A **73**, 041407R (2006)
18. L. Deslauriers, M. Acton, B.B. Blinov, K.-A. Brickman, P.C. Haljan, W.K. Hensinger, D. Hucul, S. Katnik, R.N. Kohn Jr., P.J. Lee, M.J. Madsen, P. Maunz, S. Olmschenk, D.L. Moehring, D. Stick, J. Sterk, M. Yeo, K.C. Younge, C. Monroe, Phys. Rev. A **74**, 063421 (2006)
19. G.R. De Voe, C. Kurtsiefer, Phys. Rev. A **65**, 063407 (2002)
20. A. Diaspro (ed.), *Confocal and Two-Photon Microscopy: Foundations, Applications and Advances* (Wiley-VCH, Weinheim, 2001). ISBN0-471-40920-0
21. Sami-ul-Haq, S. Mahmood, N. Amin, Y. Jamil, R. Ali, M.A. Baig, J. Phys. B, At. Mol. Opt. Phys. **39**, 1587–1596 (2006) and references therein
22. M.A. Baig, M. Yaseen, R. Ali, A. Nadeem, S.A. Bhatti, Chem. Phys. Lett. **296**, 403–408 (1998)
23. A.N. Nesmeyanov, in *Vapour Pressure of the Elements* (Infosearch, London, 1963), pp. 185–187
24. J.D. Prestage, G.J. Dick, L. Maleki, J. Appl. Phys. **66**, 1013 (1989)
25. P.K. Gosh, J.D. Prestage, G.J. Dick, L. Maleki, *Ion Traps* (Clarendon, Oxford, 1995)
26. D.J. Berkeland, J.D. Miller, J.C. Bergquist, W.M. Itano, D.J. Wineland, J. Appl. Phys. **83**, 5025 (1998)
27. M. Drewsen, A. Brønner, Phys. Rev. A **62**, 045401 (2000)
28. <http://www.simion.com/>
29. M. Vedel, J. Rocher, M. Knoop, F. Vedel, Appl. Phys. B **66**, 191–196 (1998)
30. L. Guidoni, S. Guibal, T. Coudreau, B. Dubost, F. Grosshans, J. Phys. IV Fr. **135**, 315–316 (2006)
31. M. Madine, H.W. van der Hart, J. Phys. B, At. Mol. Opt. Phys. **38**, 1895–1905 (2005)
32. R. Blümel, J.M. Chen, E. Peik, W. Quint, W. Schleich, Y.R. Shen, H. Walther, Nature **334**, 309 (1988)
33. T. Coudreau, F. Grosshans, S. Guibal, L. Guidoni, J. Phys. B, At. Mol. Opt. Phys. **40**, 413 (2007)